# Bio-Inspired All-Organic Soft Actuator Based on a $\pi$–$\pi$ Stacked 3D Ionic Network Membrane and Ultra-Fast Solution Processing

*Ravi Kumar Cheedarala, Jin-Han Jeon, Chang-Doo Kee, and Il-Kwon Oh**

**Next generation electronic products, such as wearable electronics, flexible displays, and smart mobile phones, will require the use of unprecedented electroactive soft actuators for haptic and stimuli-responsive devices and space-saving bio-mimetic actuation. Here, a bio-inspired all-organic soft actuator with a $\pi$–$\pi$ stacked and 3D ionic networked membrane based on naphthalene-tetracarboxylic dianhydride (Ntda) and sulfonated polyimide block copolymers (SPI) is presented, utilizing an ultra-fast solution process. The $\pi$–$\pi$ stacked and self-assembled 3D ionic networked membrane with continuous and interconnected ion transport nanochannels is synthesized by introducing simple and strong atomic level regio-specific interactions of hydrophilic and hydrophobic SPI co-blocks with cations and anions in the ionic liquid. Furthermore, a facile and ultrafast all-solution process involving solvent blending, dry casting, and solvent dropping is developed to produce electro-active soft actuators with highly conductive polyethylenedioxythiophene (PEDOT):polystyrenesulfonate (PSS) electrodes. Ionic conductivity and ion exchange capacity of the $\pi$–$\pi$ stacked Ntda-SPI membrane can be increased up to 3.1 times and 3.4 times of conventional SPI, respectively, resulting in a 3.2 times larger bending actuation. The developed bio-inspired soft actuator is a good candidate for satisfying the tight requirements of next generation soft electronic devices due to its key benefits such as low operating voltage and comparatively large strains, as well as quick response and facile processability.**

## 1. Introduction

Electro-kinetic bio-inspired soft actuators based on ionic conducting polymers can be a strong candidate for satisfying the tight requirements of next generation electronics such as wearable electronics, flexible displays, and smart mobile phones due to their key benefits, which include low operating voltage and comparatively large strains, as well as quick response and facile processability.[1–4] In particular, an ionic polymer-metal composite (IPMC) actuator is one of the most widely investigated artificial muscles, and can be constructed from a core ion-conductive electrolyte, and mobile molten ionic salts, sandwiched between metallic gold or platinum electrodes. Their electro-mechanical motion occurs through the redistribution of different-size mobile ions towards oppositely charged electrodes under an applied electric field.[5] High-performance IPMC actuators are functionally designed to have hydrophilic nanochannels, a micro-/nanomorphology network in a polymer matrix, highly conductive molten ionic salts, and flexible electrode materials.[6–8]

For realizing dry-type ionic polymer actuators,[9] conventional Nafion-based IPMCs incorporating ionic liquids and platinum electrodes have been reported,[10] but they still suffer from significant drawbacks, such as low actuation bandwidth, relatively low durability, environmental unfriendliness, and high cost, which limits their practical applications. To overcome these problems, alternative novel polymer actuators have been investigated to fulfill the above requirements. In particular, great effort has been invested in the development of alternative novel ionic polymers to replace Nafion, such as sulfonated aromatic and aliphatic polymers.[11] However, these still have problems to satisfy the desired electro-chemo-mechanical properties including ionic conductivity, ion exchange capacity, water/ionic liquid uptake, tensile modulus, and strength to deliver actuation performances beyond those of Nafion.[12]

Recently, the use of a sulfonated block copolymer containing hydrophilic nanochannels and a well-organized nanostructure network with a mico-/nanomorphology has been proposed to enhance the actuator performance.[13–16] Unfortunately, these sulfonated block copolymer membranes are expensive to produce due to their complex synthesis. Therefore, an alternative simple synthetic approach is needed for developing high-performance actuators using sulfonated block copolymers. Sulfonated polyimide block copolymers (SPI) contain alternate hydrophobic and hydrophilic multiblocks, and display several superior

Dr. R. K. Cheedarala, J.-H. Jeon, Prof. I. K. Oh
School of Mechanical
Aerospace and Systems Engineering
Korea Advanced Institute of Science
and Technology (KAIST)
291 Daehak-ro, Yuseong-gu, Daejeon 305–701,
Republic of Korea
E-mail: ikoh@kaist.ac.kr
Prof. C.-D. Kee
School of Mechanical Systems Engineering
Chonnam National University
300 Yongbong-dong, Buk-gu, Gwang-Ju 500-757, Republic of Korea

**DOI: 10.1002/adfm.201401136**

qualities, such as film forming capability, long shelf life, and electro-chemo-mechanical properties. They are expected to provide a special physical morphology, having more mechanical integrity and limited solvent swelling, due to the presence of sulfonic acid groups within the ionic network. Although several groups have used a series of SPI ionomers for high-performance fuel cell applications,[17,18] so far they have not been applied for electro-active polymers. Our group very recently developed an in-situ self-metallized SPI electro-active polymer actuator, but it showed moderately good electro-active performance and poor durability, which inspired us to further investigate high-performance electro-active polymers.[19] Also, Watanabe et al. have developed printable polymer actuators from a combination of ionic liquid, polyimide and carbon materials, for high actuation at low input voltage.[20] Until now, SPI-based artificial muscles, which have low actuation performance and inferior durability due to densely packed polymer matrix and low compatibility with metallic electrodes, have not been improved.

In order to develop an economically viable, highly endurable, and air-working ionic artificial muscle, we designed a $\pi$–$\pi$ stacked and self-assembled 3D ionic networked membrane with continuous and interconnected ion transport nanochannels by using simple and strong atom level regio-specific interaction of hydrophilic and hydrophobic SPI co-blocks with cations and anions in the ionic liquid. Also, we presented a simple, but ultra-fast three-step synthesis including solvent blending, dry casting and drop casting for a high-performance bio-inspired all-organic soft actuator as shown in **Scheme 1**. The actuator consists of a $\pi$–$\pi$ stacked and 3D networked Ntda-SPI ionic membrane, 1-ethyl-3-methylimidazolium bis(trifluoromethylsulfonyl)imide [EMI.$Tf_2N$] ionic liquid (IL) as the mobile electrolyte and polyethylenedioxythiophene (PEDOT):polystyrenesulfonate (PSS) as a non-metallic conducting electrode. Atom level regio-specific interaction of cations and anions in ionic liquid with hydrophilic-hydrophobic co-blocks of SPI matrix is utilized for constructing a self-assembled 3D networked polymer with continuous and interconnected ion transport nanochannels for high-performance bio-inspired all-organic soft actuator. This is suitable for moderate degree of sulfonation (DOS) for good hydrophilicity; high ion exchange capacity; high thermal stability; strong ionic interactions of hydrophilic and hydrophobic SPI co-blocks with the ionic liquid; and an organic PEDOT:PSS electrode that maintains superior mechanical strength and flexibility. Also, since the IL can act as a bridge electrolytic

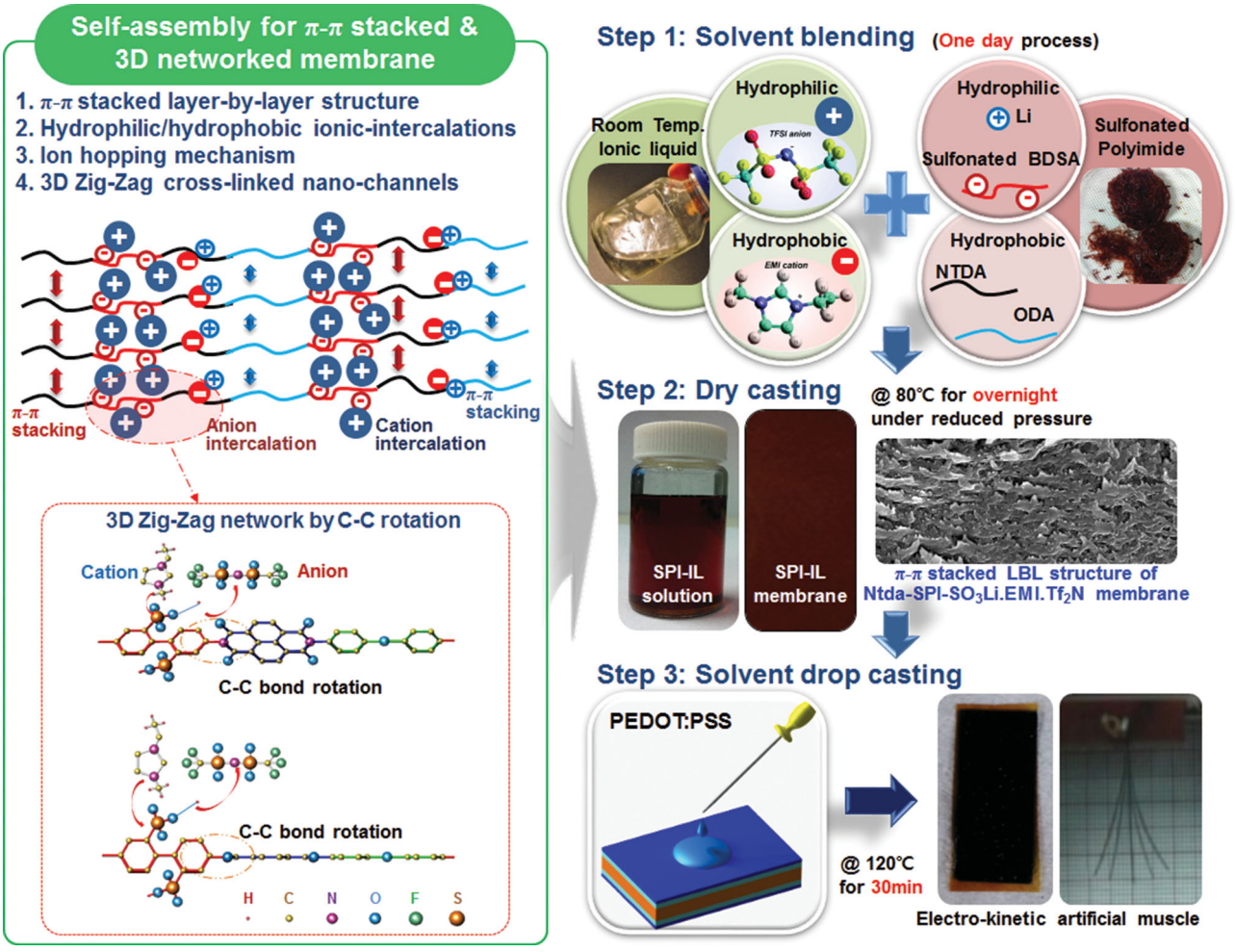


**Scheme 1.** Schematic illustration of a bio-inspired all-organic soft actuator based on a $\pi$–$\pi$ stacked 3D ionic network membrane and fabricated using an ultra-fast solution process.

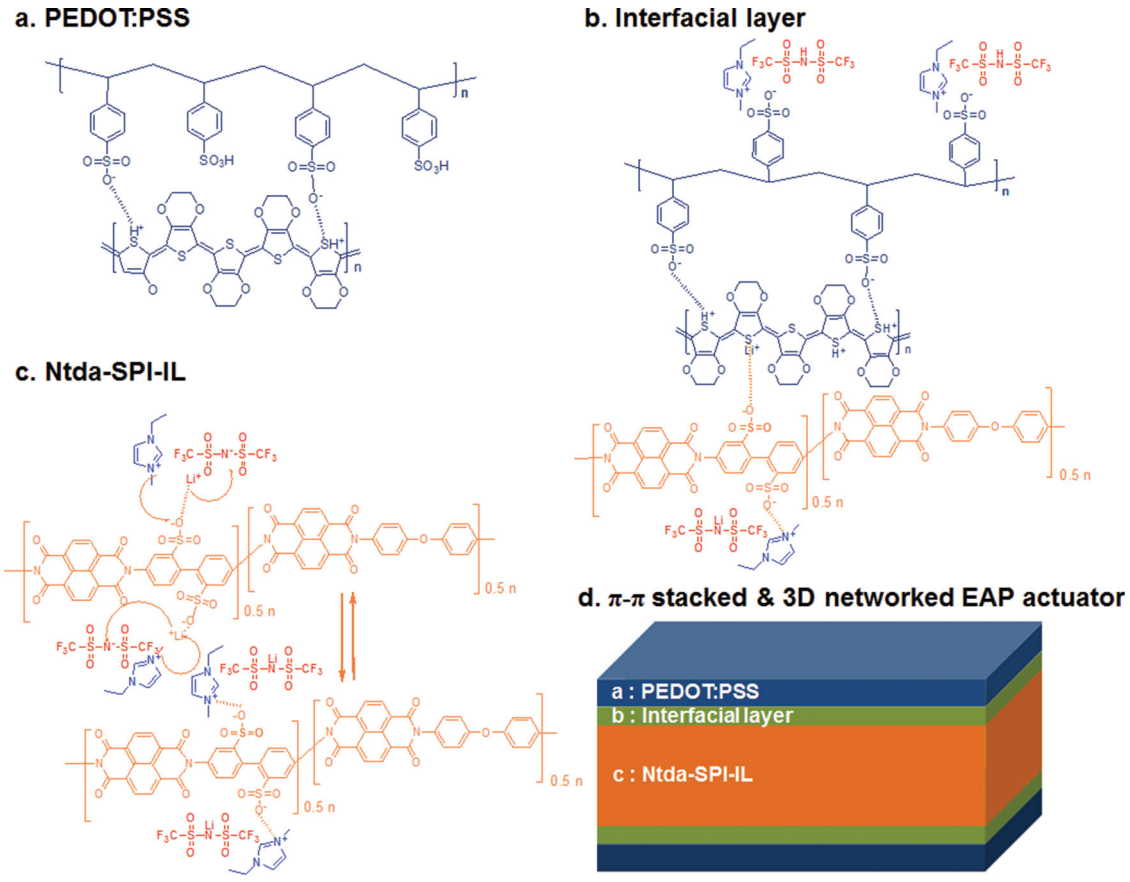


**Scheme 2.** Chemical structures and interactions inside an all-organic Ntda-SPI-IL actuator; a) chemical structure of the PEDOT:PSS electrode layer, b) chemical interactions at the interfacial layer between Ntda-SPI-IL and PEDOT:PSS, c) Ntda-SPI-IL ionic polymer, and d) layer-by-layer structure of the all-organic soft actuator.

solvent between the core SPI polymer and PEDOT:PSS electrodes, it can provide a further significant increment of actuation performance and long shelf life. Recently, Lee et al.,[18] Deligoz et al.,[21] and Ye et al.[22] independently and extensively studied the interaction of SPI membranes with imidazolium cations from various ionic liquids, but they focused only on fuel cell applications. With their inspiration, we were motivated here to use a hydrophobic ionic liquid for developing high-performance electro-active polymer actuators by producing fast ion-hopping phenomenon between cations and hydrophilic $SO_3^-$ groups and hydrophobic-hydrophobic interaction by $\pi$–$\pi$ stacking. The formation of 3D self-assembled random "in-plane" and "out of plane" nanochannels, which are generated by C-C bond rotation, the charge transfer complex (CTC), and ionic liquid interactions, can allow ions to transport easily within the membrane, as shown in Scheme 1.

Recently, interest has been growing in the use of non-metallic electrodes such as PEDOT:PSS for a compliant and highly conducting electrode for EAP actuators. Existing metallic electrodes and fabrication methods have serious drawbacks that include mud-cracks on the metal electrode surface, low stretchability and mechanical robustness, time-consuming fabrication process, degradation of polymer electrolyte and lack of reproducibility. Thus far, Oh et al.[23] has developed a high-performance electro-active hybrid actuator based on the synergistic effects of the ion migration of dissociated ionic liquids inside the main polymer matrix, and electrochemical doping processes. Furthermore, to maximize the electro-chemo-mechanical properties of the Ntda-SPI-$SO_3$Li membrane, we used PEDOT:PSS conducting polymer as a non-metallic electrode. The PEDOT:PSS in dimethyl sulfoxide (DMSO) shows very good compatibility for gluing interlayers with Ntda-SPI membranes and strong ionic interactions at the interlayers as shown in **Scheme 2**a–c. The PEDOT:PSS and the 3D nanostructured SPI membrane come into contact and interpenetrate with each other, additionally resulting in apparent high adhesion layers. As a result, two interfacial layers between PEDOT:PSS electrodes and Ntda-SPI-IL ionic membrane appear as shown in Scheme 2d. The bonding mechanism at the interfacial layers is described in Scheme 2b. Consequently, we can say that the layer number of the all-organic soft actuator is five rather than three. In this study, surface and cross-sectional scanning electron microscopy (SEM) images of Ntda-SPI membranes reveal good dispersion of ionic liquid and randomly distributed nanochannels, respectively. And the semi-crystallinity of Ntda-SPI-IL membranes with ionic clusters at nanochannels was confirmed by X-ray diffraction (XRD), and functional group interactions were determined using Fourier transform infrared spectroscopy (FT-IR) spectroscopy. The incorporation of EMI.$Tf_2N$ enhanced multiple qualities, such as mechanical strength, stiffness and

elongation at break values, and physicochemical properties like ion exchange capacity (IEC), water uptake, and ionic conductivity, resulting in a novel high-performance 3D nanochannel networked polymer actuator that shows very large bending deformations under low input voltages in air-working condition.

## 2. Results and Discussion

### 2.1. Preparation of Ntda-SPI-$SO_3$Li-IL membrane

The preparation of Ntda-SPI-$SO_3$M and their Ntda-SPI-$SO_3$M-IL (M = H.TEA, H, Li ) composite membranes was carried out by the random addition of copolymers by a one-pot method.[24] The resulting Ntda-SPI-$SO_3$H.TEA polymer fiber generally showed fairly good solubility in DMSO. 10 wt% of Ntda-SPI-$SO_3$H.$Et_3$N fibers in DMSO was cast on a flat glass plate to get a pale orange-yellow colored membrane. Next, both Ntda-SPI-$SO_3$H fibers and membranes were obtained after a proton exchange reaction of Ntda-SPI-$SO_3$H.$Et_3$N in 1.5 N HCl. And then, a lithiation reaction was conducted using 1.5 N LiCl solution to get Ntda-SPI-$SO_3$Li fibers and membranes, simultaneously, as shown in Figure S1, Supporting Information. Ntda-SPI-$SO_3$Li fibers were dissolved in DMSO and mixed with EMI.$Tf_2$N (80 wt%) to get a homogeneous solution that was re-cast on a glass plate to get an Ntda-SPI-$SO_3$Li-EMI.$Tf_2$N composite membrane.

**Figure 1** shows the digital images of all three Ntda-SPI membranes, apparently displaying from amber to brownish black due to the formation of Ntda-SPI-$SO_3$Li from Ntda-SPI-$SO_3$H TEA organic salt. The color intensity gradually increased due to doping of the lithium cation at the sulfonic acid group of the SPI polymer. The UV absorbance of the membranes as reported in Figures 1a-c further validate the increased color intensity of the membranes; 0.86% for Ntda-SPI-$SO_3$H.TEA, 1.35% for Ntda-SPI-$SO_3$H and 3.12% for Ntda-SPI-$SO_3$Li. In addition, the colored membranes were due to the presence of a lone pair of electrons on the pendant sulfonic acid group. And also, the long chain aromatic rings can show inter and intra molecular CTC phenomena because the bulky hydrophobic naphthalene and bis-benzene groups are stacked by $\pi$–$\pi$ interactions as shown in Figure 1d. In addition, hydrophilic $SO_3$H groups interact with each other between two oligomer chains.[25–27]

### 2.2. SEM

Surface and cross-sectional SEM images of Ntda-SPI membranes as shown in **Figure 2** reveal good dispersion of ionic

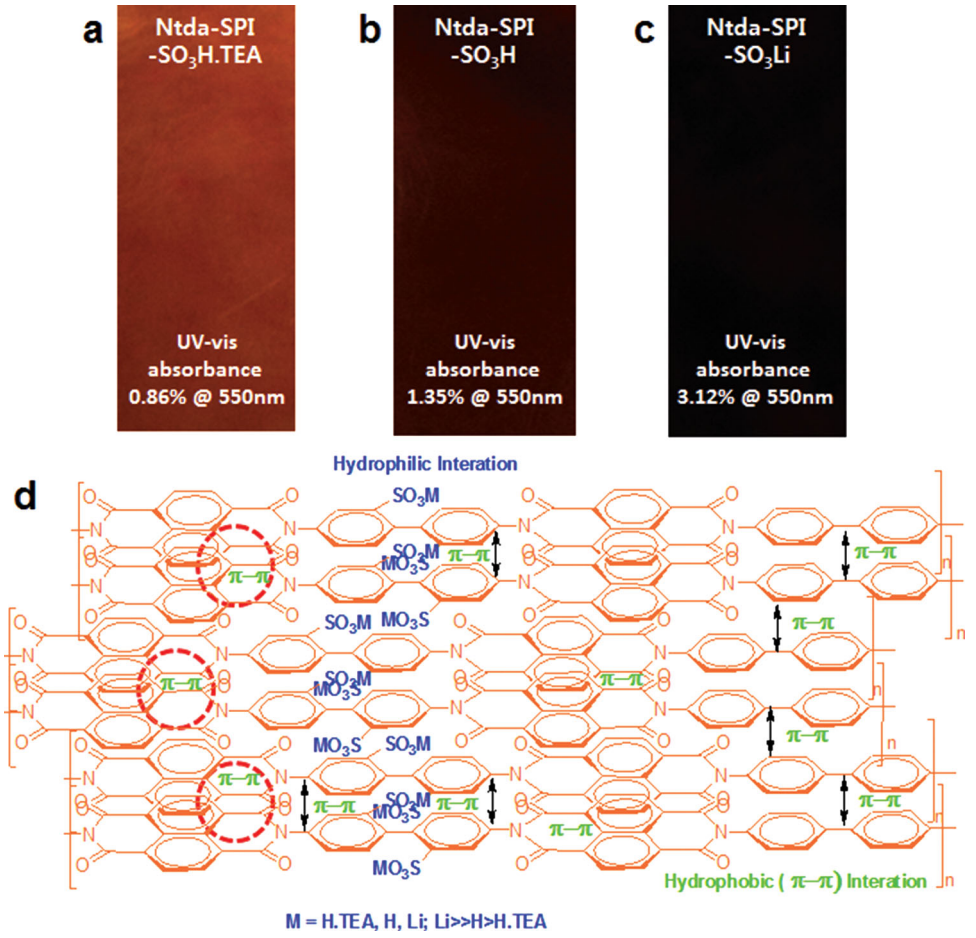


**Figure 1.** Colors of Ntda-SPI membranes and $\pi$-$\pi$ stacked polymer electrolytes integrated with ionic liquids; a) Ntda-SPI-$SO_3$H.TEA, b) Ntda-SPI-$SO_3$H, c) Ntda-SPI-$SO_3$Li, and d) $\pi$–$\pi$ stacked polymer electrolytes based on hydrophobic-hydrophobic interaction.

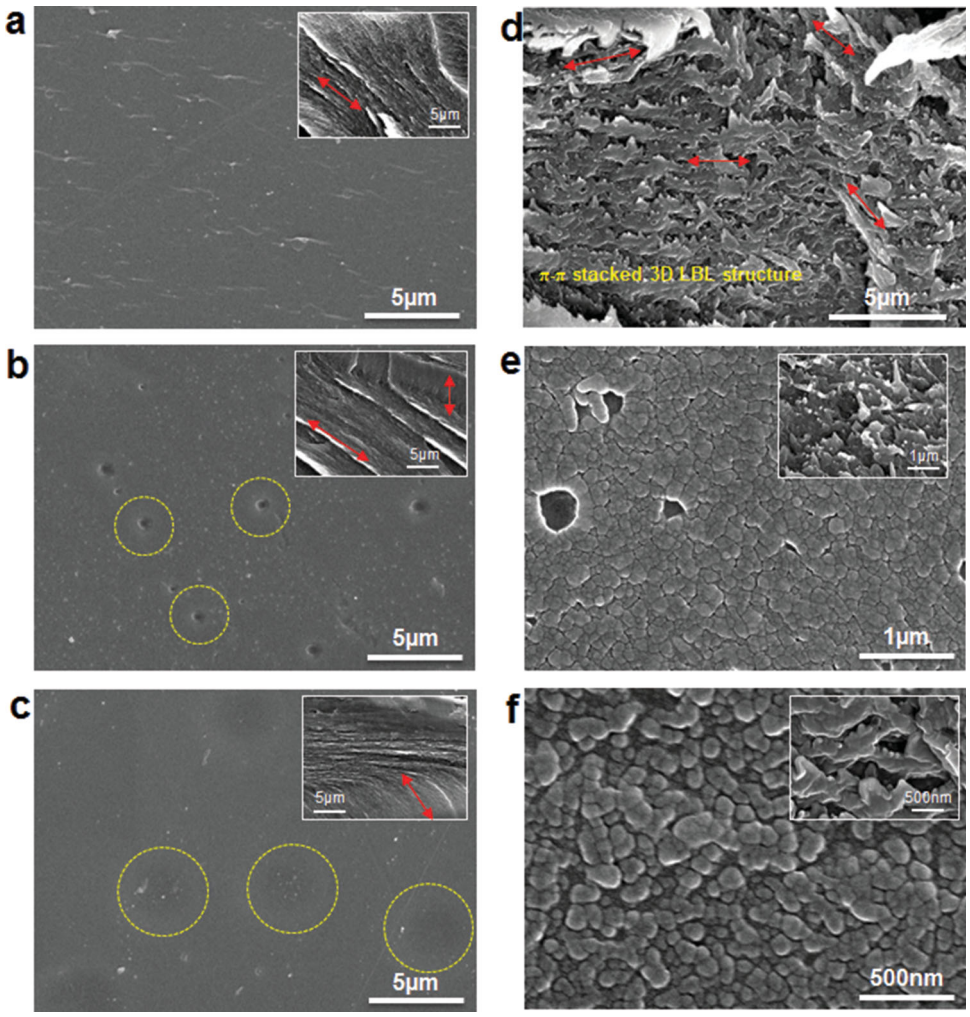


**Figure 2.** Field emission (FE)-SEM surface and cross-sectional morphologies of EMI.$Tf_2$N-Ntda-SPI- membranes; a) Ntda-SPI-$SO_3$H.TEA, b) Ntda-SPI-$SO_3$H, c) Ntda-SPI-$SO_3$Li, d) $\pi$-$\pi$ stacked 3D layer-by-layer structure, e) Ntda-SPI-$SO_3$-Li-EMI.$Tf_2$N, and f) magnified FE-SEM image of Ntda-SPI-$SO_3$-Li-EMI.$Tf_2$N.

liquid and randomly distributed nanochannels, respectively. In particular, as shown in Figure 2a, the Ntda-SPI-$SO_3$H.TEA membrane displays significant irregular micro-sized wrinkles on the surface, and densely packed and aligned nano-morphology in the cross-sectional view, due to the formation of Ntda-SPI-$SO_3$H.TEA salt. After treatment with HCl, the Ntda-SPI-$SO_3$H membrane shows irregular nano- to mico-sized pores on the surface, and loosely packed nanochannels in the cross-sectional view are observed, because of hydrolysis of the Ntda-SPI-$SO_3$H.TEA membrane, as shown in Figure 2b. After the lithiation process, there are no nano- or micro-sized pores observed on the surface of the Ntda-SPI-$SO_3$Li membrane, due to the formation of lithium cation clusters on the membrane, as shown in Figure 2c. And in the cross-sectional view, the hydrophilic and hydrophobic domains are clearly distinguished by bright beads, which represent the deposition of lithium cations.

Next, we carried out an investigation on the interaction of EMI cation and Ntda-SPI-$SO_3$Li membrane, which revealed the formation of 3D zig-zag ionic networks by a self-assembly process utilizing ionic interactions between the hydrophilic and hydrophobic domains in the Ntda- SPI-$SO_3$Li-IL polymer, as shown in Figure 2d. Also, the high-resolution surface and cross-sectional images display the formation of zig-zag channels. In particular, EMI-cations were deposited on the hydrophilic regions as bright spots which indicate clearly the formation of Ntda-SPI-$SO_3^-$.$EMI^+$ by ion exchange mechanism, as shown in Figures 2e-f. The homogenity of the blend membrane confirms the ionic interactions, which include ionic cross-linking and hydrogen-bonding between EMI-$Tf_2$N and the Ntda-SPI-$SO_3$Li membrane, resulting in the enhanced interfacial compatibility and mechanical stiffness of the composite membrane. Hydrophilic nanochannels and micro-/nano-morphology networks in polymer matrix can strongly affect the electro-chemo-mechanical properties such as IEC, ionic conductivity, and mechanical properties as listed in **Table 1** due to higher ionic interactions, higher capacitance and stronger interfacial coupling between PEDOT:PSS and 3D networked polymer matrix. Additionally, to deeply consider charge dynamics and the interface coupling, we investigated the capacitance of all three Ntda-SPI membranes with impedance analyses. The specific capacitances

**Table 1.** Electro- chemo-mechanical properties of Ntda-SPI membranes.

| Membrane | IEC (meq. $g^{-1}$) | Water/IL uptake @ RT wt% | Tensile modulus (GPa) | Tensile strength (MPa) | Elongation at break (%) | Actuation performance (strain, % @ 1.0 V, 0.1 Hz) |
|---|---|---|---|---|---|---|
| Ntda-SPI-$SO_3$H.TEA (dry) | – | – | 1.521 | 43.38 | 8.44 | – |
| Ntda-SPI-$SO_3$H.TEA (hydrated) | 0.65 | 14.5 | 1.316 | 34.73 | 11.71 | – |
| Ntda-SPI-$SO_3$H (dry) | – | – | 0.957 | 48.71 | 26.91 | – |
| Ntda-SPI-$SO_3$H (hydrated) | 2.01 | 56.5 | 0.942 | 42.21 | 30.13 | – |
| Ntda-SPI-$SO_3$Li (dry) | – | – | 1.359 | 56.87 | 19.09 | – |
| Ntda-SPI-$SO_3$Li (hydrated) | 2.23 | 55.0 | 1.308 | 53.54 | 23.59 | – |
| Ntda-SPI-$SO_3$H-TEA.IL | – | 80.0 | 1.513 | 43.96 | 25.64 | – |
| Ntda-SPI-$SO_3$H-IL | – | 80.0 | 1.299 | 48.51 | 40.34 | – |
| Ntda-SPI-$SO_3$Li-IL | – | 80.0 | 1.725 | 60.52 | 32.43 | 0.08 |
| Recast Nafion[29,30] | 0.75[29] | 16.7[29] | 0.985[29] | 13.85[29] | 10.16[29] | 0.05[30] |
| Nafion-IL[31,32] | – | 50.0[31] | 0.014[31] | – | 22.0[31] | 0.04[32] |

of Ntda-SPI-$SO_3$Li, Ntda-SPI-$SO_3$H.TEA and Ntda-SPI-$SO_3$H are measured as 177.99 μF $cm^{-2}$ (4.36 mF $g^{-1}$), 78.98 μF $cm^{-2}$ (1.82mF $g^{-1}$), and 96.19 μF $cm^{-2}$ (3.08 mF $g^{-1}$), respectively. The specific capacitance of Ntda-SPI-$SO_3$Li is superior to that of other polyelectrolyte.[28]

### 2.3. FT-IR

Functional group interactions of Ntda-SPI-$SO_3$H.TEA, Ntda-SPI-$SO_3$H and Ntda-SPI-$SO_3$Li membranes were determined using FT-IR spectroscopy as shown in **Figures 3**a–b. In particular, characteristic absorption bands appeared at 1712 $cm^{-1}$ ($\nu_{sym}$, C=O) and 1674 $cm^{-1}$ ($\nu_{asym}$, C=O), 1345 $cm^{-1}$ ($\nu$, C=C) and ($\nu$, C-N-C) corresponding to the naphthalimide ring. Also, the adsorption bands at 1247 $cm^{-1}$ ($\nu_{sym}$, O=S=O), 1081 $cm^{-1}$ ($\nu_{sym}$, O=S=O), 1025 $cm^{-1}$ ($\nu_{asym}$, O=S=O), 768 $cm^{-1}$ ($\nu_{ben}$, O=S=O) and 627 $cm^{-1}$ ($\nu_{ben}$, O=S=O) are the stretching vibrations of the $SO_2$ functional groups of the Ntda-SPI-$SO_3$H.TEA membrane.[33] The FT-IR spectrum of the Ntda-SPI-$SO_3$H membrane reveals a difference between the TEA salt and protonated membrane, the broad band at 3660–2984 $cm^{-1}$ corresponds to an OH functional group presenting from sulfonic acid. Next, the spectrum of Ntda-SPI-$SO_3$Li indicates that the new peaks are at 1198 $cm^{-1}$ (O-Li of $SO_3$Li), 1089 $cm^{-1}$ ($\nu_{asym}$, O=S=O), 1032 $cm^{-1}$ ($\nu_{asym}$, O=S=O) and 3650–3320 $cm^{-1}$ corresponding to $SO_3$-Li.

Next, the FT-IR spectrum of the Ntda-SPI-$SO_3$Li.EMI.$Tf_2N$ composite membrane was consistent with a structure composed of Ntda-SPI-$SO_3^-$.$EMI^+$ and $Tf_2N^-$.$Li^+$. The strong stretching signals of the $CF_3$ group appear at 1182 $cm^{-1}$ with a shoulder at 1225 $cm^{-1}$, and the deformation signals of the $CF_3$ group at 736 $cm^{-1}$and at 658 $cm^{-1}$ strongly support the presence of $CF_3$ in the $Tf_2N$ anion. Also, additional strong peaks appearing at 1136 $cm^{-1}$ for $SO_2$ and 1055 $cm^{-1}$ for S-N-S bond of $Tf_2N$ anion and 1348 $cm^{-1}$ with a right shoulder at 1325 $cm^{-1}$ corresponding to C=N of imidazolium cation which strongly support the presence of EMI.$Tf_2N$ in the Ntda-SPI-$SO_3$Li.IL composite membrane. As suggested in Scheme 2, the formation of ionic clusters by ultra-ionic exchange reaction between the Ntda-SPI-$SO_3$Li membrane with EMI.$Tf_2N$ is well supported by the FT-IR studies.[21] In addition, the nanochannels were developed during slow evaporation of DMSO from hydrophilic

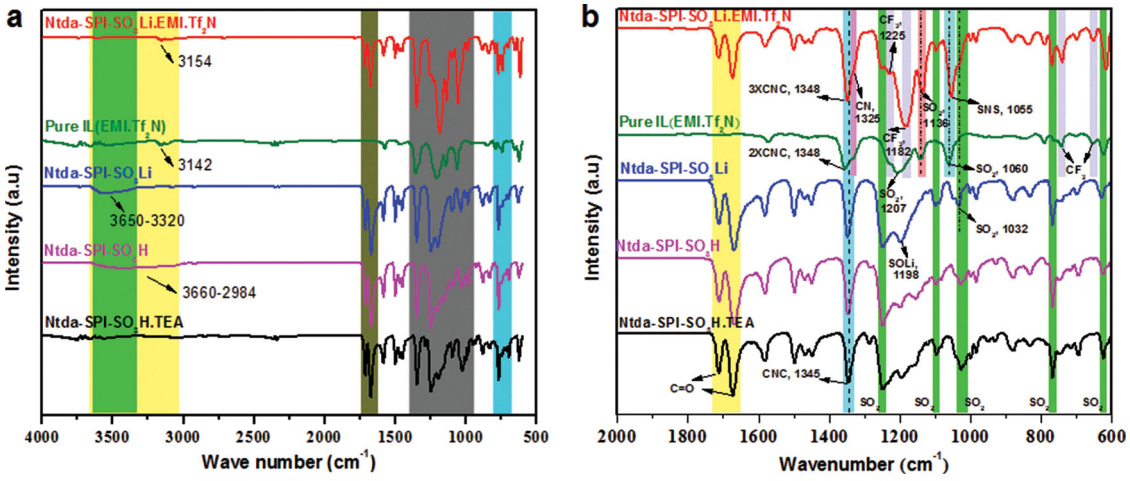


**Figure 3.** FT-IR spectra of Ntda-SPI.$SO_3$M and Ntda-SPI.$SO_3$M.EMI.$Tf_2N$ membranes in the range of a) 500 to 4000 $cm^{-1}$ and b) 600 to 2000 $cm^{-1}$.

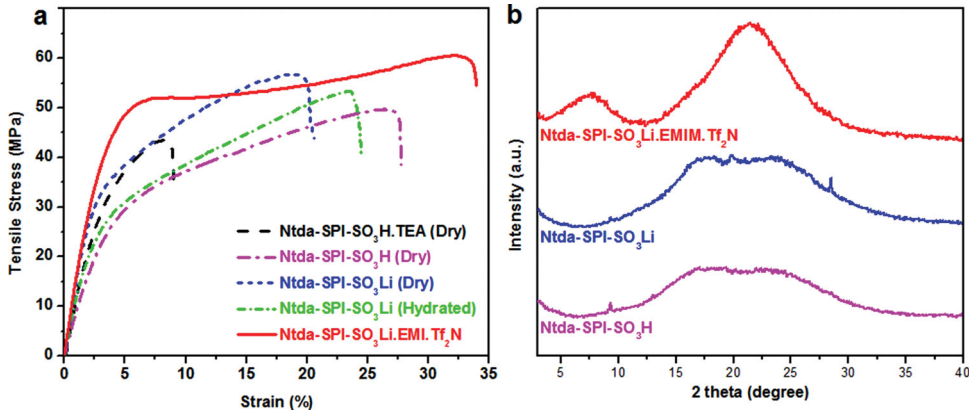


**Figure 4.** Physical properties of Ntda-SPI.$SO_3$M and Ntda-SPI.$SO_3$M.EMI.$Tf_2$N membranes: a) stress-strain curves and b) XRD patterns.

Ntda-SPI-$SO_3$Li and hydrophobic Ntda-ODA co-block polymer. Good dispersion of hydrophobic EMI.$Tf_2$N with the core Ntda-SPI polymer enhances the interfacial gluing by hydrophobic-hydrophobic and hydrophilic-hydrophilic ionic interactions, and the formation of homogeneous NTDA-$SO_3^-$.$EMI^+$-$Tf_2N^-$.$Li^+$ complex membrane, which can display high ionic conductivity, superior mechanical properties and performs as an ultra-robust biomimetic actuator.

### 2.4. Tensile Test

The mechanical stability of Ntda-SPI membranes is an important factor affecting actuator performance. To evaluate the mechanical properties of the membranes, typical tensile tests of all Ntda-SPI membranes are examined in both dry and wet conditions as shown in **Figure 4**a, and their mechanical properties are compared in Table 1. The tensile modulus of both dry and hydrated membranes decreased first from Ntda-SPI-$SO_3$H.TEA to Ntda-SPI-$SO_3$H and again increased from Ntda-SPI-$SO_3$H to the Ntda-SPI-$SO_3$Li membrane due to the formation of ionic nanochannels, caused by removing TEA groups and the subsequent formation of lithium ion clusters. In particular, the proposed composite membrane with lithium intercalation by ionic interactions displays an exceptionally superior tensile modulus, up to 1.521 GPa, which is much better than that of other SPI membranes.[22] On the other hand, the tensile modulus was measured up to 1.725 GPa for the SPI-$SO_3$Li.IL composite membrane. Thus, the consistency indicates good dispersion of EMI.$Tf_2$N in the Ntda-SPI-$SO_3$Li polymer matrix due to the chemical interactions that occurred between the sulfonic groups and EMI cations.[22] The alternating hydrophilic and hydrophobic co-block oligomer arrangement displays strong reinforcement due to ionic and $\pi$–$\pi$ interactions between the oligomer chains of the Ntda-SPI polymers. As a result, the overall tensile stiffness of the Ntda-SPI-$SO_3$Li.IL composite membrane was significantly increased due to strong ionic interactions.

### 2.5. XRD

The semi-crystallinity of Ntda-SPI-IL membranes with ionic clusters at nanochannels was confirmed by XRD as shown in Figure 4b. XRD analysis of the Ntda-SPI membranes showed some sharper peaks superimposed on the broad peaks at $2\theta$ = 5–30°, which indicates the presence of crystalline components in the amorphous membrane. However the small intensity of the peaks suggest that the amount of crystalline components are very small as compared with that of amorphous parts. The XRD pattern of the Ntda-SPI-$SO_3$H and Ntda-SPI-$SO_3$Li membranes showed a broad hallow nature without strong evident crystalline peaks, but on which sharp small peaks are superimposed, indicating the amorphous nature of the membrane.[34] The broad peaks at $2\theta$ = 16–26° strongly represent the amorphous state for common sulfonated polyimide membranes, which suggests there is further hydrophilic-hydrophobic co-block arrangement within the polymer. The Ntda-SPI-$SO_3$Li membrane shows increased crystallinity over Ntda-SPI-$SO_3$H due to the presence of Li cations.

We investigated the XRD pattern of the Ntda-SPI-$SO_3$Li.EMI.$Tf_2$N composite membrane compared with those of the Ntda-SPI-$SO_3$H and Ntda-SPI-$SO_3$Li membranes. EMI.$Tf_2$N has a plasticizing effect and it binds strongly with the Ntda-SPI-$SO_3$Li membrane to increase the crystallinity of the composite membrane.[34] The polymer used here is a random copolymer that generally does not show phase separation. There are two distinct diffraction peaks that appear as small and big sharp peaks at 22° and 7.8° providing clear evidence of the soft semi-crystalline nature of the Ntda-SPI-$SO_3$Li.EMI.$Tf_2$N membrane. The broad peaks observed in the Ntda-SPI-$SO_3$H and Ntda-SPI-$SO_3$Li membranes are changed into a sharp peak at 22° and the degree of crystallinity increased due to the formation of ionic clusters at hydrophilic co-blocks of nanochannels in the polymer.

### 2.6. IEC and Ionic Conductivity

The ion exchange capacity of the membranes plays a crucial role in evaluating water uptake and ionic conductivity. Table 1 shows the IEC values of Ntda-SPI-$SO_3$H.TEA, Ntda-SPI-$SO_3$H and Ntda-SPI-$SO_3$Li membranes. The IEC values of the Ntda-SPI-$SO_3$H.TEA, Ntda-SPI-$SO_3$H and Ntda-SPI-$SO_3$Li membranes were measured to be 0.65, 2.01, and 2.23 meq. $g^{-1}$, respectively, because $H^+$ ions are easily exchanged with $Na^+$ cations rather than the $Li^+$ cation in the Ntda-SPI-$SO_3$Li

membrane.[35] The water uptake values of Ntda-SPI-$SO_3H$. TEA, Ntda-SPI-$SO_3H$, and Ntda-SPI-$SO_3Li$ were measured to be 14.5%, 56.5%, and 55.0%, respectively.[35] The anomalous behavior was shown due to the free availability of $SO_3H$ and $SO_3Li$ groups to the water. Importantly, the ionic conductivity and mechanical stability of Ntda-based SPI membranes are strongly related to the presence of water molecules. However, excessive swelling of ionic membranes due to abundent water uptake will lead to the loss of mechanical strength, which limits the practical applications of the developed actuators. So, an ionic liquid was used in this study instead of water molecules to overcome those types of limitations by inducing strong ionic interactions and increasing mechanical stiffness and strength. Additionally, the TGA analysis strongly supports the $\pi$–$\pi$ stacking and interfacial interactions of the alternate or regular hydrophilic and hydrophobic co-blocks with ionic liquid (Figure S2, Supporting Information). Significantly, the proposed 3D networked polymer showed enhanced IEC, uptake ratio, mechanical properties, and bending performance as compared to the other ionic actuators [29–32] as listed in Table 1.

First, we compared the ionic conductivities of Ntda-SPI-IL membranes upon incorporating 80 wt% EMI.$Tf_2N$ with that of fully hydrated Ntda-SPI membranes, as shown in **Figure 5**a. The fully hydrated Ntda-SPI-$SO_3H$ membrane exhibits higher ionic conductivity compared to the Ntda-SPI-$SO_3Li$ and Ntda-SPI-$SO_3H$-TEA membranes due to the higher affinity between $SO_3H$ and water molecules in the form of the hydronium ion ($H_3O^+$). On the other hand, the self-assembled 3D networked Ntda-SPI-$SO_3Li$-IL membranes show better ionic conductivity values ($\approx 1.20–3.22 \times 10^{-4}$ S cm$^{-1}$) at room temperature condition (20–30 °C) than that of the Ntda-SPI-$SO_3H$- and Ntda-SPI-$SO_3H$-TEA-IL membranes ($\approx 0.51–1.63 \times 10^{-5}$ S cm$^{-1}$). In the Ntda-SPI-$SO_3H$-IL membrane, the -$SO_3H$ groups promote the dissociation of ionic liquids, compared with the Ntda-SPI-$SO_3H$-TEA-IL membrane, where ionic conductivity is hindered by TEA salt. The regular 3D nanochannels of the Ntda-SPI-$SO_3Li$-IL membrane shown in Figures 2d-f result in enhanced ionic conductivity, which is attributed to these ionophilic regions formed around the Li ionic cluster of side chains ($SO_3Li$), and also leads to increased ionic liquid absorption, helping easy and fast ion transport within the membrane, thereby offering the capability to improve actuation performance.

### 2.7. Actuation Performance

Figure 5b shows the time-dependent bending responses of the actuators based on the Ntda-SPI- $SO_3$-Li, -H, -H.TEA incorporating ionic liquid (EMI.$Tf_2N$) under sinusoidal electrical input with ± 2.5 V peaks and 0.1 Hz frequency. In particular, the peak-to-peak strain of the Ntda-SPI-$SO_3Li$-EMI.$Tf_2N$ actuator reaches up to 0.26%, which is 3.2 times more than the Ntda-SPI-$SO_3H$-TEA actuator of 0.08%. This higher bending performance of the newly developed actuator is induced by the high ionic conductivity and tuned mechanical properties, resulting from strong ionic interactions among the $SO_3Li$, ionic liquid and PEDOT:PSS, and $\pi$–$\pi$ stacked 3D networked polymer matrix.

Additionally, peak-to-peak displacements were measured along with the strain under sinusoidal electrical wave from ± 0.5 to 2.0 V peaks at 0.01, 0.05 and 0.1 Hz frequencies and are shown in Figure 5c. The degree of electromechanical deformation is roughly affected by the applied voltage and frequency, because ionic mobility is highly dependent on the electric potential field in the polymer matrix. The large peak-to-peak displacements, over 1.0 mm, were attained in all frequency ranges at or below ±1 V. Most importantly, the Ntda-SPI-$SO_3Li$-IL actuator exhibited a durable response without an obvious drop of actuation performance during 60 min under AC 0.5 V and 0.1 Hz as shown in Figure 5d. After an actuation test for 60 min, the actuator still exhibits very harmonic response without response distortion and performance degradation as shown in the inset of Figure 5d. It is thought that the synergistic effects of its unique 3D ionic networked structure and the strong ionic interaction between the IL, sulfonic acid groups in 3D nanochannels and DMSO-doped PEDOT:PSS could effectively prevent the degradation of actuation performance resulting from leakage of ionic liquid and Faradaic behavior.[32,36] Figure 5e shows the large deformed shapes with constant curvature of the Ntda-SPI-$SO_3$-Li-IL actuator under electrical harmonic input with magnitude of 3.0 V and excitation frequency of 0.1 Hz.

## 3. Conclusions

We have demonstrated a self-assembled 3D ionic networked polymer actuator based on Ntda-SPI-$SO_3Li$-IL with $\pi$–$\pi$ stacked layers and alternate hydrophilic nanochannels, resulting in superior electro-chemo-mechanical properties and actuation performance. Well-arranged hydrophilic sulfonic groups have good compatibility with both PEDOT:PSS and EMI.$Tf_2N$ at an atomic level within the Ntda-based SPI membrane, thereby providing continuous and interconnected ionic transport paths through ionic nanochannels, reducing electrochemical resistance and tuning desired electro-chemo-mechanical properties to enhance actuation performance and durability. The Ntda-SPI-$SO_3Li$-IL membrane showed a dramatic increment of the tensile modulus, up to 131%, and tensile strength, up to 174%, and elongation at break values up to 277%, respectively, as compared to its starting membrane (hydrated Ntda-SPI-$SO_3H$.TEA). In addition, the enhanced protonation and uptake of ionic liquid in the Ntda-SPI-$SO_3Li$ polymer membrane, resulting from the ionic interaction of the sulfonic acid of the SPI matrix and imidazolium cations of IL, resulted in higher IEC and ionic conductivity. These synergistic effects were beneficial in designing a high-performance ionic actuator which shows large bending deformation under harmonic electric inputs, as compared with the original Ntda-SPI-$SO_3H$.TEA and Ntda-SPI-$SO_3H$ polymer membranes incorporating ionic liquid. In particular, the Ntda-SPI-$SO_3Li$ ionic polymer actuator with EMI.$Tf_2N$ sandwiched between the PEDOT:PSS electrodes exhibited an actuation strain of more than 0.3% under 2.0 V with fast actuation. The present results also suggest that the controlled self-assembly process for a hydrophilic-hydrophobic co-block ionic polymer with strong ionic interactions and ion transport nanochannels can be used for tailoring the actuation performance of electrokinetic ionic polymer actuators, which are required for the next generation electronic products such as wearable soft electronics, flexible displays, and smart mobile phones.

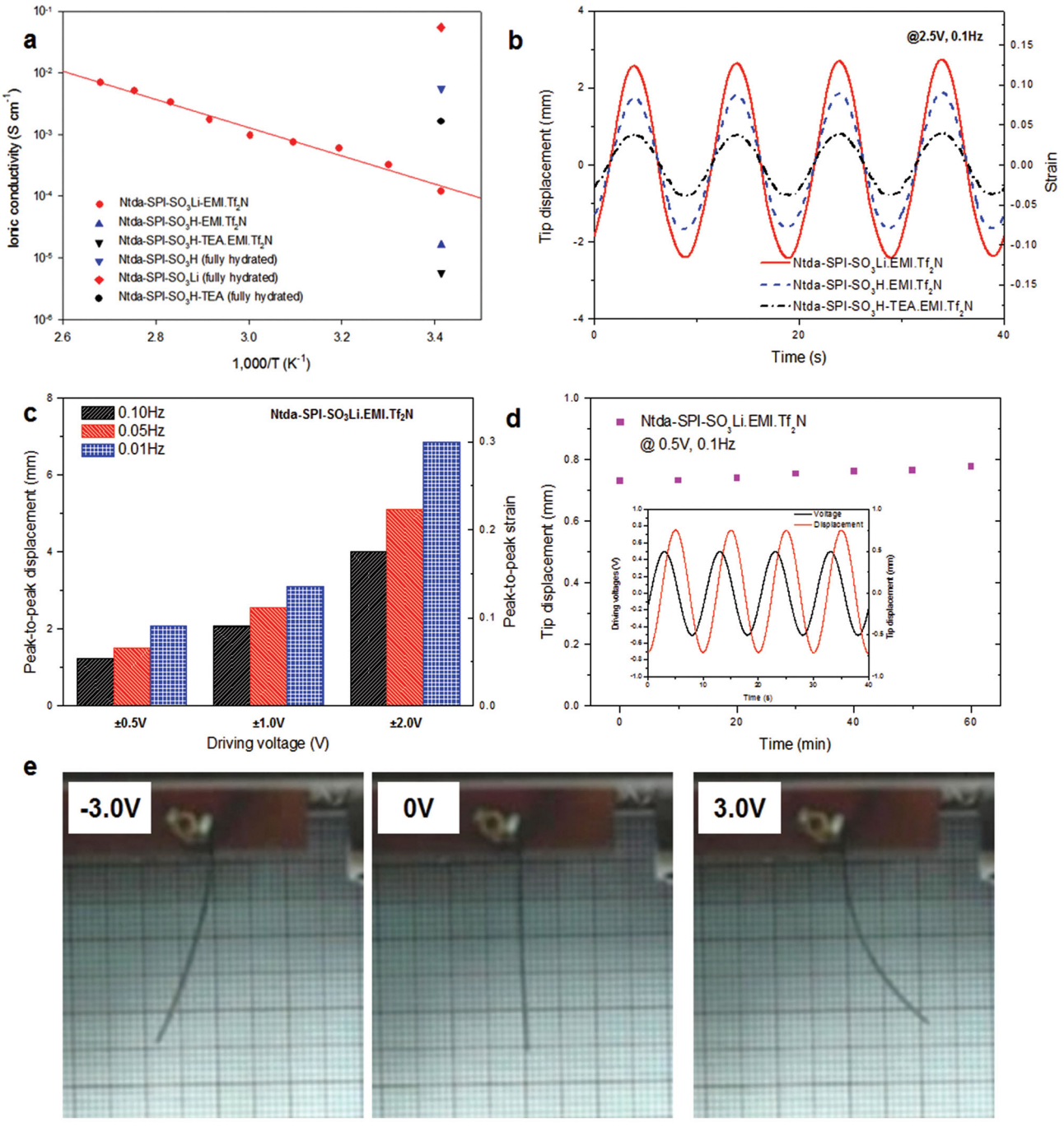


**Figure 5.** Ionic conductivity and actuation performances of Ntda.SPI.$SO_3$Li-EMI.$Tf_2$N actuator membranes; a) ionic conductivity, b) harmonic responses under sinusoidal input with peak voltage of 2.5 V and excitation frequency of 0.1 Hz, c) peak-to-peak displacements at different voltages and frequencies, d) durability results, and e) deformed shapes of the developed actuator.

## 4. Experimental Section

*Materials*: 1,4,5,8-Naphthalene tetracarboxylic dianhydride (Ntda) (90%, Aldrich) was soaked in dimethylformamide (DMF) while stirring at 60 °C for 12 h. After filtration, Ntda was washed with acetone and dried in a vacuum. 2,2'-bendizine sulfonic acid (BDSA) (70%, Tokyo Kasei) was washed with deionized (DI) water and dissolved in DI water by adding triethyl amine. Acidification with 1 M $H_2SO_4$ (aq) afforded the precipitation of pure BDSA. 4,4′-diaminodiphenyl ether (ODA, Sigma–Aldrich), Ntda, and BDSA were dried in an oven at 90 °C for overnight. Benzoic acid, *m*-cresol, and lithium chloride (LiCl) from Sigma–Aldrich were used as-received. 1-ethyl-3-methylimidazolium bis(trifluoromethylsulfonyl)imide [EMI.$Tf_2$N], 99% purity, ionic liquid were used as-received from IOLITEC GmbH, Heilbronn, Germany. Triethylamine ($Et_3$N, Sigma–Aldrich) was distilled and dried with 4 Å molecular sieves prior to use. The conducting polymer PEDOT:PSS is commercially available in the form of a water dispersion (Baytron P AG, H C starck, 1.3 wt% dispersion in water).

*Synthesis of Ntda-SPI.$SO_3$H.TEA Co-Polyimide Fibers*: The preparation of Ntda-SPI-$SO_3$H.TEA co-polyimide membrane with ≈50% degree of sulfonation (DOS) was conducted. To a 100 mL completely dried 3-neck flask were added 2.0 g (5.8 mmol) of BDSA, 15.0 mL of *m*-cresol and 3 ml (3.6 mmol) of TEA successively under nitrogen flow with stirring at room temperature. After BDSA was completely dissolved, 3.116 g (11.6 mmol) of NTDA, 1.16 g (5.8 mmol) of ODA and 1.51 g (2.2 mmol) of benzoic acid were added. The mixture was stirred at room temperature for a few minutes, and then heated at 80 °C for 4 h and 180 °C for 20 h. After cooling to 100 °C, an additional 20 mL of *m*-cresol was added to dilute the highly viscous solution, which was then poured into 300 mL of acetone. The fiber-like yellow precipitate was filtered off, washed with acetone and dried in vacuum.

*Synthesis of Ntda-SPI.$SO_3$Li Fibers*: Ntda-SPI.$SO_3$H.TEA co-polyimide fibers were initially treated with 1 N HCl for 12 h to get the Ntda-SPI.$SO_3$H form and washed with DI water. Next, Ntda-SPI.$SO_3$H fibers were lithiated using 1.5 N LiCl solution for about 12 h, then washed with DI water to get Ntda-SPI.$SO_3$Li fibers as shown in Figure S1, Supporting Information.

*Synthesis of Ntda-SPI.$SO_3^-$ $EMI^+.Tf_2N^-.H^+$Composite Membrane*: Ntda-SPI.$SO_3^-$ $EMI^+.Tf_2N^-.H^+$ membrane was prepared by solution mixing method. 2 g of Ntda-SPI.$SO_3$Li fibers were dissolved in DMSO (15 mL) and 1.6 g of EMI.$Tf_2$N was added. The reaction mixture was stirred for 12 h to get a homogeneous solution, later cast on a glass plate and evaporated at 90 °C for 24 h to obtain a composite membrane with a thickness of 80 μm.

*Fabrication of the PEDOT:PSS-Ntda-SPI.$SO_3$Li-EMI.$Tf_2$N-PEDOT:PSS Composite Ionic Polymer Actuator*: Self-assembled layer-by-layer sandwiched PEDOT:PSS-Ntda-SPI.$SO_3$Li-EMI.$Tf_2$N-PEDOT:PSS membrane was fabricated by ultra-fast all-solution process. 5 wt% of DMSO was added into the aqueous PEDOT:PSS commercial solution at RT. The PEDOT:PSS homogeneous solution was dropped uniformly on the pre-cast Ntda-SPI.$SO_3$Li-EMI.$Tf_2$N membrane using a dropper and dried at 120 °C for 30 min. The same procedure was repeated to the other side of the membrane to get a composite actuator.

*SEM, FT-IR and XRD*: SEM observations were carried out on an FEI Sirion FESEM, 30 kV microscope. The membranes were thoroughly dried before capturing the images and surface morphology and cross sectional images were studied. The FT-IR spectra of the Ntda-SPI.$SO_3$H.TEA, Ntda-SPI.$SO_3$H and Ntda-SPI.$SO_3$Li membranes were scanned using an IFS66V/S & HYPERION 3000, Bruker Optiks (Germany). XRD of the membranes are measured using a DMAX-Ultima III X-ray diffractometer in the range of 3 to 40°.

*Tensile-Stress Curves and Thermogravimetric Analysis*: The tensile strength, modulus properties and elongation of the Ntda-SPI.$SO_3$H.TEA, Ntda-SPI.$SO_3$H, Ntda-SPI.$SO_3$Li and Ntda-SPI.$SO_3$Li.EMI.$Tf_2$N membranes were determined using a table-top universal testing machine (AGS-5kNX, Shimadzu Corp., Japan.) equipped with a 1 kN load cell. The test speed was set to a rate of 10 mm/min. The cross sectional area of the membrane samples was measured before testing with a micrometer. The gauge length between the grips was 10 mm. All tested samples had a regular rectangular shape. TGA measurements of the Ntda-SPI.$SO_3$H.TEA, Ntda-SPI.$SO_3$H, Ntda-SPI.$SO_3$Li and Ntda-SPI.$SO_3$Li.EMI.$Tf_2$N membranes were done on a Thermogravimetric Analyzer (TG209F3) from NETZSCH (Germany), over temperatures ranging between 40 °C and 800 °C under a nitrogen atmosphere condition and at a heating rate of 10 °C $min^{-1}$. All membranes were air dried.[9]

*Water Uptake Ratio*: The electromechanical response of ionic polymer actuators depends on the structure of the polymer backbone, ionic conductivity, and level of hydration. Water uptake values of the Ntda-SPI membranes were determined according to the ASTM D 570-98 (2010) el – standard test method for water absorption of plastics. Three pieces each of the Ntda-$SO_3$H.TEA, Ntda-$SO_3$H and Ntda-$SO_3$Li membranes were prepared using the following steps: initially, membranes were heated at 110 °C for 1 h and then at 50 °C for 24 h in a hot air oven, then the membranes were cooled down to RT, weighed immediately and then soaked in deionized water at RT for 24 h. The membranes were removed, gently wiped with tissue paper, and weighed again for the final weight. The water uptake (WU) ratio of the membranes was calculated using the following equation.

$$\text{Water uptake} = \frac{W_{wet} - W_{dry}}{W_{dry}} \times 100 \quad (1)$$

where $W_{dry}$ is the weight of the dry membrane and $W_{wet}$ is the weight of the water-swollen membrane.

*Electrochemical Properties*: IEC indicates the number of mill equivalents of ions in 1.0 g each of the dry Ntda-SPI.$SO_3$H.TEA, Ntda-SPI.$SO_3$H and of Ntda-SPI.$SO_3$Li membranes. To determine the IEC, the titration method was applied, using phenolphthalein as an indicator. The acidic form of the membrane was converted to the sodium form by immersion in 1 M NaCl solutions for 24 h. The exchanged ions in the solution were titrated with a 0.1 M NaOH solution. The IEC values were determined by the following equation:

$$\text{IEC} = \frac{\text{Consumed NaOH (mL)} \times \text{molarity of NaOH}}{\text{Weight of membrane}} \quad (2)$$

The ionic conductivities of the ionic liquid doped Ntda-SPI.$SO_3$H.TEA, Ntda-SPI.$SO_3$H and of the Ntda-SPI.$SO_3$Li membranes were calculated through the electrochemical impedance spectroscopy data obtained from a complex impedance analyzer (VersaSTAT 3 potentiostat/galvanostat, Princeton Applied Research) over a frequency range of 10–1 MHz under a maximum voltage of 20 mV. Membranes of a circular shape with a 6 mm diameter and an ECC-STD electrochemical cell (EL-CELL) with two stainless steel electrodes were used. The ionic conductivity can be calculated with the following equation:

$$\text{Ionic conductivity} = \frac{1}{R(\Omega)} \times \frac{L(cm)}{S(cm^2)} [S/cm] \quad (3)$$

where R is the ionic resistance, i.e., charge transfer resistance, which is calculated from the intercept of the semicircle at the low-frequency side of the Nyquist plot with the real axis, and L and S are the thickness and area of the membranes.

*Setup for Actuation Tests*: The size of the actuator was 4 mm × 30 mm × 0.1 mm. The actuator was clamped using about a 4 mm × 5 mm area at one end. The experimental setup for the measurement of actuation consisted of a PXI 6252 data acquisition board, a current amplifier (UPM1503, Quanser), a charged-couple device camera (XCHR50, Sony) and a laser displacement sensor (LK-031, Keyence). All the data were acquired and controlled by an NI-PXI system (1042Q, NI) by using the LabVIEW program. The strain generated in the actuator was estimated by the following equations.

$$\varepsilon = 2d\delta/(l^2 + \delta^2) \quad (4)$$

where $d$, $\delta$, and $l$ are the thickness, the tip displacement and the free length of the actuator.

## Supporting Information

Supporting Information is available from the Wiley Online Library or from the author.

## Acknowledgements

R.K.C. and J.H.J. contributed equally to this work. This work was supported by a National Research Foundation of Korea Grant funded by the Korean Government (No. 2012R1A2A2A01047543).

Received: April 9, 2014
Revised: May 13, 2014
Published online: July 25, 2014

[1] T. F. Otero, E. Angulo, J. Rodríguez, C. Santamaría, *J. Electroanal. Chem.* **1992**, *341*, 369.
[2] F. Engelhardt, G. Ebert, R. Funk, *Adv. Mater.* **1992**, *4*, 227.
[3] Y. Osada, H. Okuzaki, H. Hori, *Nature* **1992**, *355*, 242.
[4] S. Mohsen, J. K. Kwang, *Smart Mater. Struct.* **2001**, *10*, 819.
[5] J. Lu, S. G. Kim, S. Lee, I. K. Oh, *Adv. Funct. Mater.* **2008**, *18*, 1290.
[6] B. J. Akle, M. D. Bennett, D. J. Leo, *Sens. Actuators, A* **2006**, *126*, 173.
[7] J. H. Jeon, S. P. Kang, S. Lee, I. K. Oh, *Sens. Actuators, B* **2009**, *143*, 357.
[8] M. Rajagopalan, I. K. Oh, *ACS Nano* **2011**, *5*, 2248.
[9] J. H. Jeon, R. K. Cheedarala, C. D. Kee, I. K. Oh, *Adv. Funct. Mater.* **2013**, *23*, 6007.
[10] J. W. Lee, Y. T. Yoo, *Sens. Actuators, B* **2009**, *137*, 539.
[11] J. W. Lee, S. M. Hong, J. Kim, C. M. Koo, *Sens. Actuators, B* **2012**, *162*, 369.
[12] C. Jo, D. Pugal, I. K. Oh, K. J. Kim, K. Asaka, *Prog. Polym. Sci.* **2013**, *38*, 1037.
[13] S. Imaizumi, H. Kokubo, M. Watanabe, *Macromolecules* **2013**, *45*, 401.
[14] R. Gao, D. Wang, J. R. Heflin, T. E. Long, *J. Mater. Chem.* **2012**, *22*, 13473.
[15] P. H. Vargantwar, K. E. Roskov, T. K. Ghosh, R. J. Spontak, *Macromol. Rapid Commun.* **2012**, *33*, 61.
[16] X. L. Wang, I. K. Oh, J. Lu, J. Ju, S. Lee, *Mater. Lett.* **2007**, *61*, 5117.
[17] N. Asano, M. Aoki, S. Suzuki, K. Miyatake, H. Uchida, M. Watanabe, *J. Am. Chem. Soc.* **2006**, *128*, 1762.
[18] S. Y. Lee, A. Ogawa, M. Kanno, H. Nakamoto, T. Yasuda, M. Watanabe, *J. Am. Chem. Soc.* **2010**, *132*, 9764.
[19] J. Song, J. H. Jeon, I. K. Oh, K. C. Park, *Macromol. Rapid Commun.* **2011**, *32*, 1583.
[20] S. Imaizumi, Y. Ohtsuki, T. Yasuda, H. Kokubo, M. Watanabe, *ACS Appl. Mater. Interfaces* **2013**, *5*, 6307.
[21] H. Deligoez, M. Yilmazoglu, *J. Power Sources* **2011**, *196*, 3496.
[22] Y. S. Ye, C. Y. Tseng, W. C. Shen, J. S. Wang, K. J. Chen, M. Y. Cheng, J. Rick, Y. J. Huang, F. C. Chang, B. J. Hwang, *J. Mater. Chem.* **2013**, *21*, 10448.
[23] S. S. Kim, J. H. Jeon, S. D. Kee, I. K. Oh, *Smart Mater. Struct.* **2013**, *22*, 085026.
[24] C. Genies, R. Mercier, B. Sillion, N. Cornet, G. Gebel, M. Pineri, *Polymer* **2001**, *42*, 359.
[25] R. Watari, M. Nishihara, H. Tajiri, H. Otsuka, A. Takahara, *Polym. J.* **2013**, *45*, 839.
[26] M. J. Rashkin, M. L. Waters, *J. Am. Chem. Soc.* **2002**, *124*, 1860.
[27] N. J. Heaton, P. Bello, B. Herradón, A. del Campo, J. Jiménez-Barbero, *J. Am. Chem. Soc.* **1998**, *120*, 12371.
[28] H. Okuzaki, S. Takagi, F. Hishiki, R. Tanigawa, *Sens. Actuators, B* **2014**, *194*, 59.
[29] J. H. Jung, V. Sridhar, I. K. Oh, *Compos. Sci. Technol.* **2010**, *70*, 584.
[30] J. H. Jung, J. H. Jeon, V. Sridhar, I. K. Oh, *Carbon* **2011**, *49*, 1279.
[31] K. Kikuchi, S. Tsuchitani, *J. Appl. Phys.* **2009**, *106*, 053519.
[32] J. W. Lee, S. Yu, S. M. Hong, C. M. Koo, *J. Mater. Chem. C* **2013**, *1*, 3784.
[33] C. Y. Tseng, Y. S. Ye, J. Joseph, K. Y. Kao, J. Rick, S. L. Huang, B. J. Hwang, *J. Power Sources* **2011**, *196*, 3470.
[34] A. Inoue, W. Zhang, T. Tsurui, A. R. Yavari, A. L. Greer, *Philos. Mag. Lett.* **2005**, *85*, 221.
[35] X. Guo, J. Fang, T. Watari, K. Tanaka, H. Kita, K. I. Okamoto, *Macromolecules* **2002**, *35*, 6707.
[36] J. Kim, J. H. Jeon, H. J. Kim, H. Lim, I. K. Oh, *ACS Nano* **2014**, *8*, 2986.